Transport in ITER-like plasmas in neoclassical, fluid and gyrokinetic descriptions

J. Candy[1], H. Nordman[2], T. Fülöp[2] and E. Belli[1]

[1] General Atomics, San Diego, CA
[2] Chalmers University of Technology, Göteborg, Sweden

e-mail contact of main author: candy@fusion.gat.com

Abstract. Turbulent and neoclassical transport in a reference hybrid-mode ITER plasmas is studied using a hierarchy of modeling tools. Transport from ITG/TEM instability is studied with nonlinear gyrokinetic simulations and compared with results from quasilinear fluid and gyro-Landau fluid models. Simulations include full kinetic ion and electron dynamics, although a pure-D mixture is assumed for the bulk ions. We perform the comparison over the full region interior to the pedestal, and derive all simulation parameters from the reference profiles. These comparisons form the starting point for future predictive modeling using direct gyrokinetic simulations. For reference, neoclassical transport of particles and energy is also computed using a new first-principles kinetic code with an advanced multi-species collision operator. Both quasilinear models tend to stay roughly within a factor of two of the reference gyrokinetic simulations, which is remarkable given that they are at least four orders of magnitude faster than direct nonlinear simulation.

1. Introduction

Current performance predictions for ITER are based on transport modeling using reduced models for the core thermal and particle transport. The reasoning is that, for both the neoclassical and turbulent contributions to the transport, the fundamental equations are far too expensive to simulate via nonlinear gyrokinetics when a steady-state solution is sought. Thus, improved performance modeling for ITER will require either more accurate reduced models or direct gyrokinetic (and neoclassical) simulation. The purpose of the present work is to begin moving in the direction of direct kinetic simulation for predictive modeling. This is still an enormously formidable prospect, mainly because the cost of direct nonlinear gyrokinetic simulation is at least four orders of magnitude higher than even the most complex of reduced models. Thus, to start with, we need to leverage reduced transport models as much as possible in a direct approach to modeling. Recently a new reduced model, TGLF, has been developed [1, 2] and incorporates various improvements over its predecessor, GLF23 [3]. In this work we compare the transport coefficients obtained from GYRO [4], TGLF [1] and a quasilinear fluid model (which we denote here as QFM) [5, 6] for realistic ITER profiles. The practical intent of this comparison is to gauge the accuracy limitations of TGLF and QFM in comparison to the more fundamental (and expensive) nonlinear simulations.

GYRO is a nonlinear gyrokinetic code with both local and global operational modes. It has electromagnetic capability, plasma shaping effects via Miller geometry, pitch-angle collisions and can simulate a full or partial torus. It has been in full production use since about 2003. TGLF is a theory-based quasilinear transport model which uses 12 moments for passing particles and 3 for trapped particles. The closure coefficients depend on the trapped fraction, making TGLF significantly more complicated than GLF23 [3]. Finally,
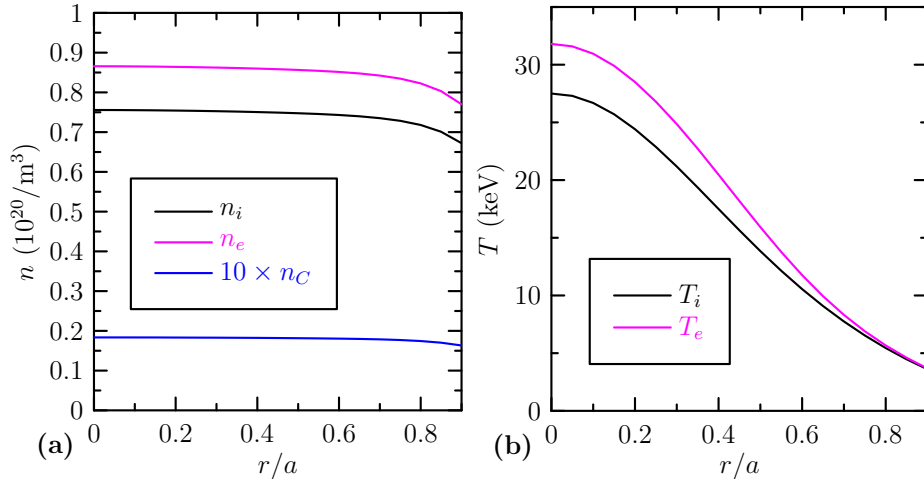
FIG. 1. ITER reference (a) density and (b) temperature profiles.

in the QFM model a set of fluid equations is used to compute the turbulent particle and energy fluxes. The model considers moment equations for perturbations in density, parallel velocity and pressure for ions, impurities and trapped electrons. The quasilinear expressions for the fluxes in QFM are derived by fixing the spatial scale of the turbulence by choosing $k_r \rho_s = k_\theta \rho_s = 0.2$, and an eigenvalue equation is solved for the general mode width (see Ref. [5] and references therein). Results from TGLF and QFM do not require massive computational resources, and are therefore more convenient for parameter scans and for profile prediction purposes.

2. Simulation Methodology

In the past, GYRO-TGLF comparisons have been reported [2] as have GYRO-QFM comparisons [5]. This is the first work to make a collective comparison, and to focus on reactor-relevant parameters over the entire minor radius inside the pedestal. The GYRO [4] simulations discussed herein used a $(L_x, L_y)/\rho_s = (128, 96)$ perpendicular domain with 128 velocity-space points, 180 radial gridpoints and 16 complex toroidal modes, and 10/20 points per passing/trapped orbit. The wavenumber range resolved was $0 \leq k_\theta \rho_s \leq 1$, which is about 25% higher than "standard" ITG/TEM resolution, but still neglects a possible high-k contribution from ETG turbulence [7]. Kinetic electron and plasma shaping effects were retained in all simulations, but only the Poisson equation was solved, threreby limiting the fluctuations to electrostatic. The same physics (kinetic electrons, shape, electrostatic, etc) was retained in TGLF, whereas QFM results are based on circular geometry. Collisional effects were also neglected in all turbulent transport calculations. Simulation parameters are derived from ITER reference profiles [8] used in previous GYRO comparisons with QFM [5]. This is a hybrid scenario obtained with the ASTRA code using a 12 MA plasma current, a 5.2 T magnetic field, a 6.2 m major and 2 m minor radius. The temperature and density profiles are plotted in Fig. 1, with additional local dimensionless parameters (required for code input) summarized in Tables 1 and 2. Especially in the region $r/a < 0.5$, these parameters give rise to transport which is closer to threshold than that normally studied in parameter scans (see Ref. [9], for example). In Table 1, r is the midplane minor radius, q is the safety factor, s is the magnetic shear, κ is the elongation, $s_\kappa \doteq (r/\kappa)d\kappa/dr$, δ is the triangularity, $s_\delta = rd\delta/dr$ and Δ is the

Table 1. Local geometrical parameters for ITER reference equilibrium

r	q	s	κ	s_κ	δ	s_δ	Δ
0	1.006	0.023	1.416	0	0	0	0
0.1	1.045	-0.027	1.422	0.001	0.008	0.031	-0.265
0.2	1.031	-0.01	1.418	-0.005	0.028	0.073	-0.256
0.3	1.011	-0.08	1.413	-0.015	0.036	-0.012	-0.241
0.4	1.016	0.2	1.409	-0.005	0.048	0.09	-0.222
0.5	1.113	0.664	1.412	0.026	0.051	0.001	-0.2
0.6	1.314	1.182	1.426	0.095	0.077	0.204	-0.172
0.7	1.643	1.746	1.458	0.196	0.108	0.078	-0.139
0.8	2.166	2.452	1.511	0.372	0.152	0.867	-0.099
0.9	3.08	3.771	1.604	0.723	0.235	1.603	-0.052

Table 2. Local profile parameters for ITER reference equilibrium

r	n_C/n_e	T_i/T_e	a/L_{ne}	a/L_{nC}	a/L_{Te}	a/L_{Ti}	B_{unit}	$(a/c_s)\tau_{ei}^{-1}$
0	0.021	0.865	0	0	0	0	7.106	0.0018
0.1	0.021	0.862	0.008	0.023	0.552	0.608	7.136	0.0019
0.2	0.021	0.857	0.016	0.019	1.104	1.166	7.124	0.0022
0.3	0.021	0.852	0.024	0.031	1.647	1.675	7.142	0.0028
0.4	0.021	0.855	0.038	0.031	2.23	2.135	7.15	0.0041
0.5	0.021	0.869	0.05	0.064	2.789	2.535	7.412	0.0067
0.6	0.021	0.897	0.076	0.085	3.247	2.902	7.781	0.0120
0.7	0.021	0.932	0.149	0.158	3.661	3.3	8.625	0.0232
0.8	0.021	0.961	0.362	0.377	4.017	3.78	9.598	0.0478
0.9	0.021	0.981	1.129	1.125	4.796	4.548	11.738	0.1039

Shafranov shift. In Table 2, B_{unit} is the effective magnetic field and τ_{ei}^{-1} is the electron-ion collision rate (for reference, the latter quantities are defined in Ref. [10]). We define two variations of the ITER scenario: first the "baseline" (B) case, which neglects impurities and sets n_i equal to n_e, and second, the "impurity" (I) case which retains the finite carbon ($Z = 6$, $A = 12$) fraction, n_C.

We also remark that the local GYRO [4] simulations reported here were carried out using the TGYRO transport manager, which automates, compresses and summarizes an entire radial scan over (in this case) 9 distinct radial locations, $r = (0.1, 0.2, \ldots, 0.9)$, into a single TGYRO simulation. Such a scan, with three kinetic species (electrons, deuterium and carbon), took only 14 hours on 1152 cores of the ORNL Cray XT4.

For neoclassical fluxes, we show results derived from the newly-developed NEO code [10], which performs a direct solution of the fundamental drift-kinetic equation using the zeroth-order Hirshman-Sigmar (HS0) collision operator [11]. We have used the HS0 operator rather than the full operator since only the former behaves correctly when $T_e \neq T_i$. Although neoclassical transport in ITER is relatively weak owing to the low collisionality, the neoclassical ion energy flux will nevertheless have some effect on the shape of the modeled ion and impurity profiles near the magnetic axis (in the case where no additional physics, such as sawtooth mixing, is considered).
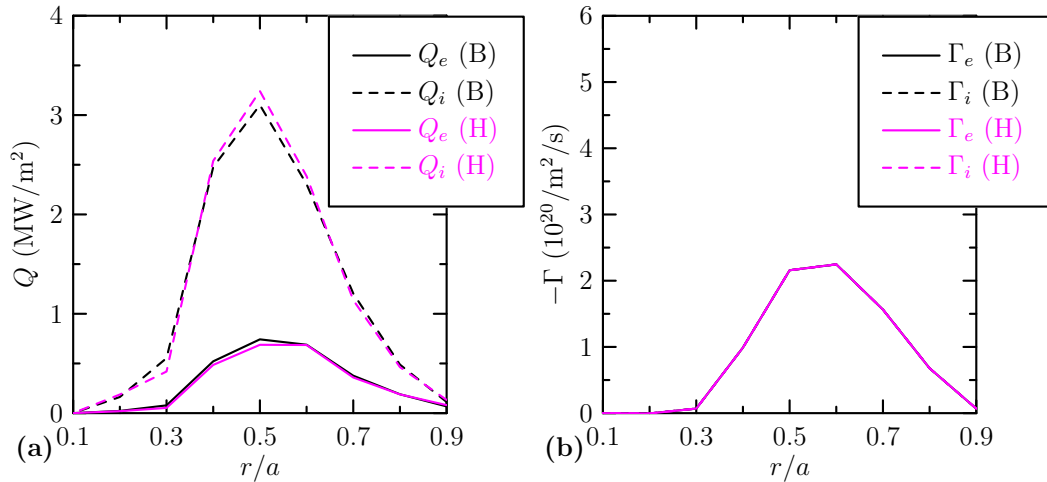
FIG. 2. Electron and ion (a) energy and (b) particle fluxes for baseline (black) and high-resolution (magenta) GYRO simulations. This demonstrates that the GYRO simulations are insensitive to increased velocity-space resolution. Note that all particle fluxes are equal in part (b) as a consequence of quasineutrality.

3. Results

First, as a check on GYRO convergence, we ran standard (B) and high-resolution (H) variants of the baseline case. In comparison to B, the H-case has 1.6 times the poloidal resolution, and 1.875 times the velocity-space resolution, for a total factor of 3 increase in resolution. The result, shown in Fig. 2, indicates that GYRO is sufficiently well-converged at the given spatial domain size and wavenumber resolution. In what follows, we give a complete breakdown of the matrix of transport coefficients in physical, rather than local gyroBohm (GB), units. We will discuss the implications of this choice of normalization later.

In the most important channels, the ion and electron energy flux, we observe very good agreement between TGLF and GYRO at outer radii, but a significant discrepancy at inner radii, as shown in Fig. 3. The QFM curves in Fig. 3 show resonable agreement with GYRO at outer radii, yet manage to reproduce the transition to low transport at inner radii. The same trends are observed in the carbon and total energy fluxes plotted in Fig. 4. In the case of particle fluxes, as shown in Fig. 5, again TGLF matches well at outer radii, but significantly overpredicts at interior radii. While QFM uniformly underpredicts the tranport, it more closely matches the qualitative shape of the transport tail at inner radii. This is in some sense accidental considering that plasma shaping effects are absent from QFM. We remark also that the simulated per-particle carbon particle and energy fluxes are roughly the same as for the primary ions in all cases.

A unique feature of these results is that the parameter regime defined by the ASTRA equilibrium is significantly closer to threshold than what is normally chosen for gyrokinetic parameter scans. This perhaps magnifies the difficulty of matching GYRO results with a quasilinear model, particularly in the region $r/a < 0.5$ where the onset of a Dimits shift (i.e., a flow-dominated regime) appears as the profiles flatten and the plasma approaches marginal stability. Needless to say, more comparisons are required to further clarify these issues.

A useful measure of the overall agreement is obtained by computing the volume average
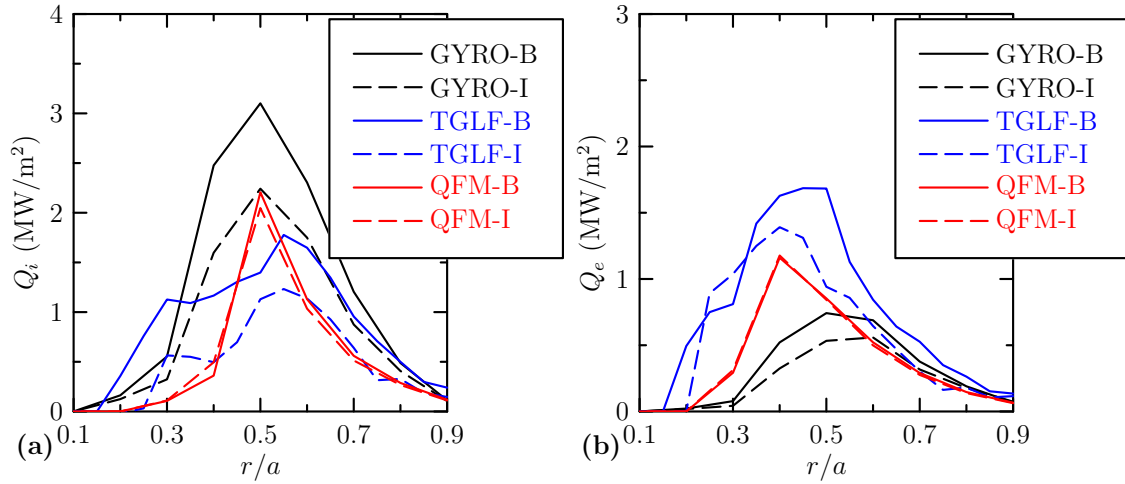
FIG. 3. (a) Ion and (b) electron energy flux for GYRO (black), TGLF (blue) and QFM (red). The baseline case (solid curves) and impurity case (dashed curves) are also compared.
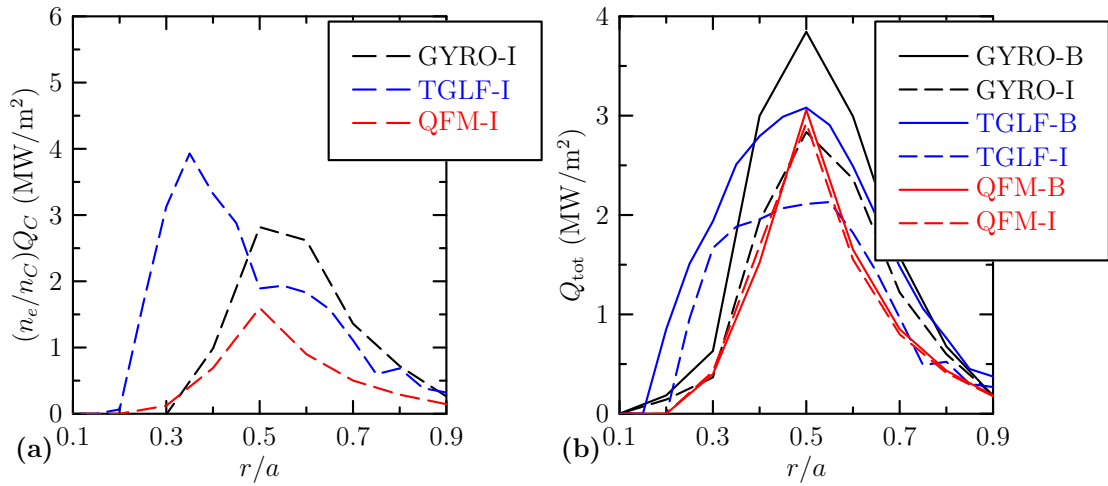

FIG. 4. (a) Carbon and (b) total energy flux for GYRO (black), TGLF (blue) and QFM (red). The baseline case (solid curves) and impurity case (dashed curves) are also compared.

Table 3. Volume-averaged accuracy of reduced models

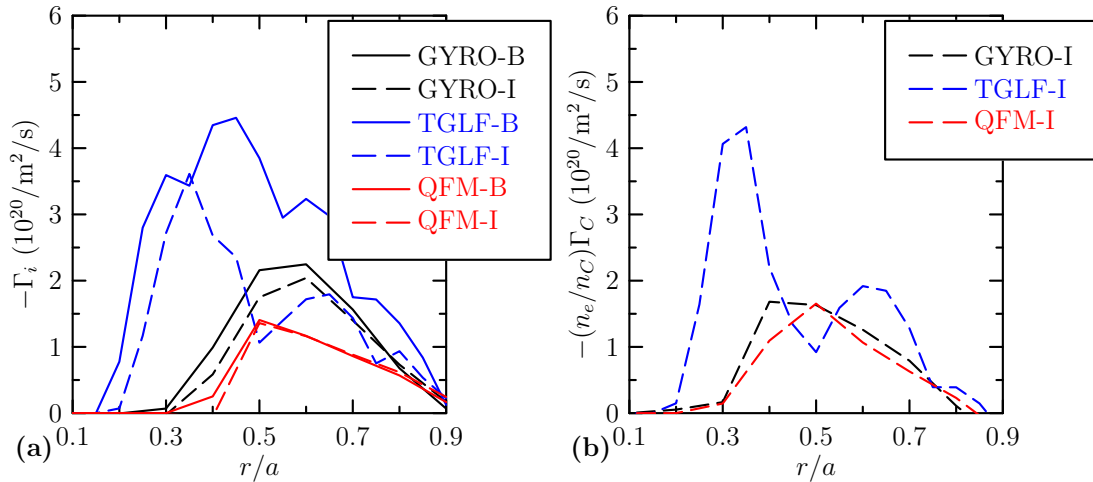|	$x = $ QFM	$x = $ TGLF
$\langle \Gamma_i^x \rangle / \langle \Gamma_i^{\mathrm{GYRO}} \rangle$	0.63	1.39
$\langle \Gamma_C^x \rangle / \langle \Gamma_C^{\mathrm{GYRO}} \rangle$	0.87	1.69
$\langle \Gamma_e^x \rangle / \langle \Gamma_e^{\mathrm{GYRO}} \rangle$	0.65	1.41
$\langle Q_i^x \rangle / \langle Q_i^{\mathrm{GYRO}} \rangle$	0.63	0.58
$\langle Q_C^x \rangle / \langle Q_C^{\mathrm{GYRO}} \rangle$	0.46	1.18
$\langle Q_e^x \rangle / \langle Q_e^{\mathrm{GYRO}} \rangle$	1.43	1.94
$\langle Q_{\mathrm{tot}}^x \rangle / \langle Q_{\mathrm{tot}}^{\mathrm{GYRO}} \rangle$	0.80	0.89

FIG. 5. (a) Ion and (b) carbon particle fluxes for GYRO (black), TGLF (blue) and QFM (red). The baseline case (solid curves) and impurity case (dashed curves) are also compared. Electron particle fluxes are not shown since they follow directly from quasineutrality.

of the fluxes

$$\langle Q_\sigma \rangle \doteq \frac{\int dr\, r\, Q_\sigma(r)}{\int dr\, r} \quad \text{and} \quad \langle \Gamma_\sigma \rangle \doteq \frac{\int dr\, r\, \Gamma_\sigma(r)}{\int dr\, r}\,, \tag{1}$$

where σ is the species index. Taking ratios thus yields a single number indicative of the closeness to the reference gyrokinetic value; such ratios are tabulated in Table 3

Although, to this point, we have expressed all results in physical units, gyrokinetic simulation results are more commonly expressed in *local gyroBohm units*

$$\chi_{\text{GB}} = \rho_s^2 c_s/a\,, \quad Q_{\text{GB}} = n_e(kT_e)c_s(\rho_s/a)^2 \quad \text{and} \quad \Gamma_{\text{GB}} = n_e c_s(\rho_s/a)^2\,, \tag{2}$$

since the gyrokinetic equations are intrinsically gyroBohm-scaled. Because the gyroBohm factor varies significantly over the minor radius, curves plotted in gyroBohm units look rather different than curves plotted in physical units. For example, in Fig. 6, curves of the normalized energy diffusivity, χ_i/χ_{GB}, peak strongly towards the plasma edge. Also apparent is that the sub-GB regime for electrons encompasses a significant fraction ($r/a \leq 0.5$) of the minor radius. In the sub-GB region, the standard quasilinear approach, which does not account for the nonlinear upshift (Dimits shift), is expected to overpredict the transport. This is indeed what is presently observed for TGLF. Also, QFM does a remarkably good job of matching the reference gyrokinetic simulations, despite a significant number of approximations. Note that in QFM a fixed scale for the turbulence is used whereas the nonlinear kinetic results indicate a shift of the peak of the transport spectrum towards lower mode numbers for increasing values of q, mainly due to Landau resonances, as illustrated in Fig. 7 for GYRO.

Finally, for completeness, we summarize the neoclassical transport coefficients in Fig. 8. These results were obtained by direct kinetic simulation with NEO [10] using a 3×3 collision operator with full electron-deuterium-carbon exchange terms. As expected, the neoclassical transport levels are about two order of magnitude lower than the corresponding turbulent levels.
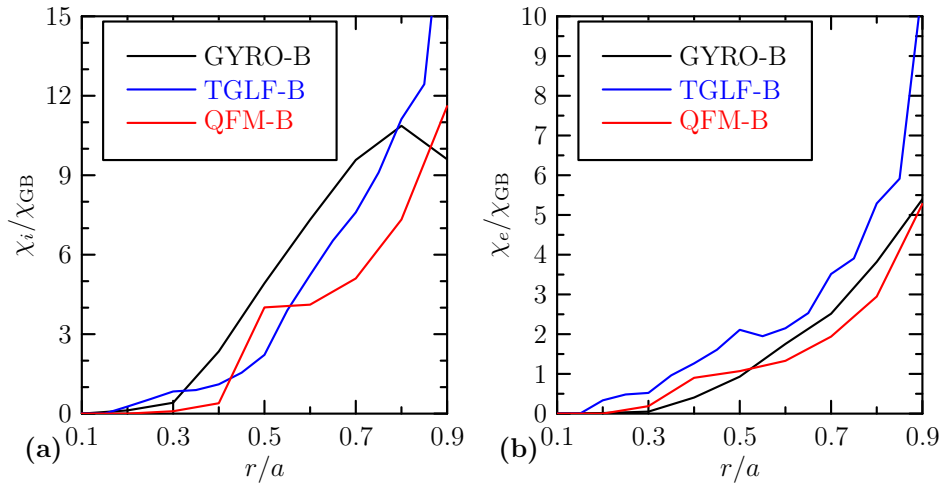
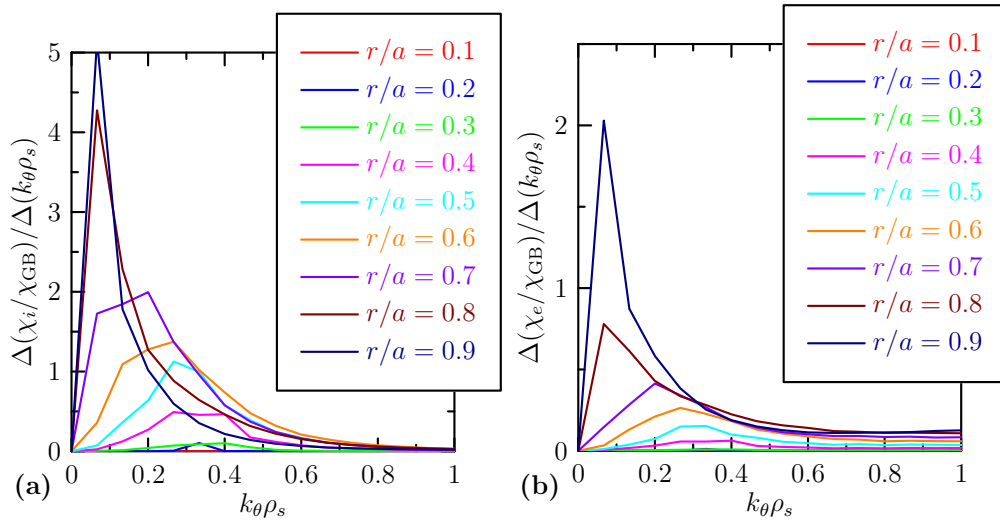FIG. 6. (a) Ion and (b) electron energy diffusivities for GYRO (black), TGLF (blue) and QFM (red).

FIG. 7. Wavenumber dependence of (a) ion and (b) electron energy diffusivities for GYRO over the domain $0.1 \leq r/a \leq 0.9$.
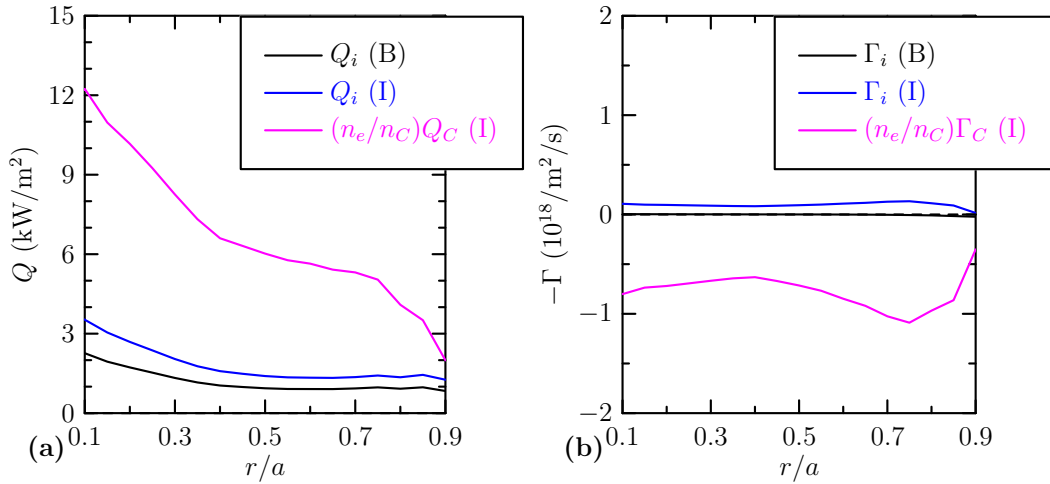
FIG. 8. *Neoclassical (a) energy and (b) particle fluxes calculated with the NEO code using a complete cross-species collision operator.*

4. Acknowledgement

References

[1] STAEBLER, G. et al., Phys. Plasmas **14** (2007) 055909.

[2] KINSEY, J. et al., Phys. Plasmas **15** (2008) 055908.

[3] WALTZ, R. et al., Phys. Plasmas **4** (1997) 2482.

[4] CANDY, J. et al., J. Comput. Phys. **186** (2003) 545.

[5] NORDMAN, H. et al., Phys. Plasmas **14** (2007) 052303.

[6] WEILAND, J., *Collective modes in inhomogeneous plasma*, IOP Bristol, 2000.

[7] CANDY, J. et al., Plasma Phys. Controlled Fusion **49** (2007) 1209.

[8] POLEVOI, A., Private communication, 2006.

[9] KINSEY, J. et al., Phys. Plasmas **14** (2007) 102306.

[10] BELLI, E. et al., Plasma Phys. Controlled Fusion **50** (2008) 095010.

[11] HIRSHMAN, S. et al., Phys. Fluids **19** (1976) 1532.